Title
Climate models miss most of the coarse dust in the atmosphere

Journal
Science Advances, 6(15)

ISSN
2375-2548

Authors
Adebiyi, Adeyemi A
Kok, Jasper F

Publication Date
2020-04-10

DOI
10.1126/sciadv.aaz9507

Peer reviewed

ATMOSPHERIC SCIENCE

Climate models miss most of the coarse dust in the atmosphere

Adeyemi A. Adebiyi* and Jasper F. Kok

Coarse mineral dust (diameter, ≥5 μm) is an important component of the Earth system that affects clouds, ocean ecosystems, and climate. Despite their significance, climate models consistently underestimate the amount of coarse dust in the atmosphere when compared to measurements. Here, we estimate the global load of coarse dust using a framework that leverages dozens of measurements of atmospheric dust size distributions. We find that the atmosphere contains 17 Tg of coarse dust, which is four times more than current climate models simulate. Our findings indicate that models deposit coarse dust out of the atmosphere too quickly. Accounting for this missing coarse dust adds a warming effect of 0.15 W·m^{-2} and increases the likelihood that dust net warms the climate system. We conclude that to properly represent the impact of dust on the Earth system, climate models must include an accurate treatment of coarse dust in the atmosphere.

INTRODUCTION

Desert dust is a key component of the Earth's climate system, accounting for ~70% of the mass and ~25% of the shortwave (SW) radiation extinguished by aerosols in the atmosphere (*1*). The impacts of dust on the Earth system, as a result of interactions with radiation, clouds, and biogeochemistry, are sensitive to the sizes of dust particles in the atmosphere (*2*). Although climate models are the primary tool used to understand dust impacts on the Earth system (*3*), several lines of evidence indicate that these climate models consistently and substantially underestimate the amount of coarse dust (with diameter $D \geq 5$ μm) in the atmosphere (*4*–*6*). This underestimation of coarse dust has been recognized since the 1970s with the detection of large dust particles over the Caribbean (*7*) that were difficult to account for in models (*8*). Recent ship-based lidar observations of dust mass concentration profiles over the North Atlantic Ocean found that measured coarse dust concentrations still exceed those simulated in several models for the same time period (*4*). In addition, several aircraft-based in situ observations have found that the measured coarse dust particles are usually larger than expected, regardless of the distance from the dust source (*5*, *9*). Moreover, observations made over the Pacific Ocean also showed that more coarse dust particles are transported further east, away from the Asian desert, than captured by models (*10*). Overall, several campaign observations have now shown that more coarse dust particles are present in the atmosphere than are accounted for in current global models (*4*–*6*), but exactly how much coarse dust is missing globally in climate models remains unclear.

Coarse dust is known to have distinct impacts on several Earth system processes (*2*). One such key impact of coarse dust is its effect on biogeochemistry and carbon sequestration (*11*). Coarse dust dominates the deposited dust mass flux (*12*) and, thus, affects the delivery of key micronutrients like iron to the ocean surface, which may in turn influence the uptake of carbon dioxide into the deep ocean (*13*). Another way coarse dust affects Earth system processes is through interactions with clouds and radiation (*14*). Coarse dust particles are more effective cloud and ice condensation nuclei than fine dust particles (diameter $D < 5$ μm) and, thus, influence the amount and spatial distribution of clouds, which in turn affect global precipitation and climate (*14*, *15*). In addition, while fine dust particles cool the climate by predominantly scattering SW radiation, coarse dust particles warm the climate system by absorbing both SW and longwave (LW) radiation (*16*). This absorption of radiation by coarse dust can also affect atmospheric stability and circulation (*17*). Since the impact of dust depends on its size, the underestimation of coarse dust in global models hinders our ability to accurately estimate the various impacts of dust on the Earth system (*2*).

To address the systematic underestimation of coarse dust in climate models (*4*, *5*), we develop an approach that determines how much coarse dust is in the atmosphere and how much of that coarse dust is missing from current climate models. Our approach uses a framework to constrain the global coarse dust loading by using published measurements of atmospheric dust size distributions, observational constraints on dust shape and global dust optical depth, and an ensemble of global model simulations. We find that the atmosphere contains four times more coarse dust than is currently simulated in models, which results in a substantial underestimation of the coarse dust impacts on the Earth system, including warming by coarse dust at the top of the atmosphere (TOA).

RESULTS AND DISCUSSION

Size distribution of the missing coarse dust

We estimate the global size distribution of atmospheric coarse dust by combining an ensemble of global atmospheric model simulations with a compilation of published in situ measurements of dust size distributions (see Materials and Methods and fig. S1). We take the compilation of previously published in situ measurements and the ensemble of global model simulations from a recent study (*18*) [the model ensemble includes Goddard Institute for Space Studies (GISS), Weather Research and Forecasting model coupled with Chemistry (WRF-Chem), Community Earth System Model (CESM), Goddard Earth Observing System coupled with Chemistry (GEOS-Chem), ARPEGE-Climate, and Integrated Massively Parallel Atmospheric Chemical Transport (IMPACT); see Materials and Methods and section S2 for details]. We determine the globally representative size-dependent correction factor needed to bring the fractional contribution of coarse dust in each model simulations in optimal agreement with

Department of Atmospheric and Oceanic Sciences, University of California, Los Angeles, Los Angeles, CA 90095, USA.
*Corresponding author. Email: aadebiyi@ucla.edu

measured coarse dust size distributions. We define our coarse dust as dust particles with a diameter between 5 and 20 μm because 5 μm represents the diameter at which most models begin to underestimate the coarse dust (*16*) and also because most models generally do not incorporate dust particles beyond 20 μm (*2*, *19*). Although dust particles larger than 20 μm have recently been measured in the atmosphere (*20*), we limit our estimate to 20 μm because measurements of dust with $D > 20$ μm are still scarce, and using them may result in a large uncertainty for the global estimate of the coarse dust (*2*). Despite limiting the coarse dust diameter to 20 μm, our result shows that coarse dust accounts for 58% [95% confidence interval (CI), 50 to 69%] of the atmospheric dust mass, which is substantially more than the 19% (6 to 31%) estimated by an ensemble of global model simulations (Fig. 1A).

To determine how accurately our estimates compare with measurements, we use a separate methodology described in (*18*) to obtain the coarse dust fractions at the locations, heights, and seasons for which over two dozen measurements of dust size distributions were taken. On the basis of the constraints on global dust size distribution (Fig. 1A), we find that our estimates of coarse dust size distributions are in excellent agreement with measurements at various locations, heights, and seasons (Figs. 1B and 2). In contrast, global models significantly underestimate the fraction of coarse dust relative to each of these measurements. On average, this systematic model underestimation of coarse dust ranges between half to one-and-a-half orders of magnitude and increases with dust diameter (Fig. 1B and table S1). Although the model bias is significant for all locations considered here, most models perform better near dust-source regions than farther downstream (Fig. 2 and table S2). We also compare our estimates of the fraction of coarse dust in the atmosphere to recent estimates by Kok *et al.* (*16*). Whereas Kok *et al.* (*16*) obtained the global fraction of coarse dust by combining constraints on the emitted dust size distribution with model simulations of dust lifetime, our approach uses direct measurements of atmospheric dust size distribution to constrain the global size distribution. Although the 43% (38 to 49%) global fraction of atmospheric coarse dust estimated by Kok *et al.* (*16*) is higher than that simulated by global models, it is still substantially lower than our estimates (Fig. 1A). Furthermore, the spatio-temporally collocated comparison with the compilation of measured dust size distributions indicates that, although the coarse dust estimates from Kok *et al.* (*16*) are in better agreement with measurements than model simulations (figs. S2 and S3), they still underestimate the coarse dust fraction in the atmosphere (Fig. 1B). Overall, the fractional contribution of coarse dust in the atmosphere per unit dust mass is higher than what is simulated in models or estimated by constraining only the emitted dust size distribution.

Atmospheric mass load of the missing coarse dust

We combined our constrained global dust size distribution (Fig. 1A) with observational constraints on global dust aerosol optical depth and dust extinction efficiency to estimate the size-resolved global atmospheric dust load—that is, the total mass load of dust in the atmosphere for each particle size (see Materials and Methods). We used constraints on the global dust aerosol optical depth from Ridley *et al.* (*21*), which combined extensive satellite and ground-based observations of aerosol optical depth with an ensemble of model simulations that separated dust from nondust optical depth. We also used constraints on the size-resolved dust extinction efficiency from Kok *et al.* (*16*), which leveraged observational and experimental constraints on dust shape and dust index of refraction. This study, thus, accounted for the effect of dust asphericity, which enhances dust extinction by ~30% in the SW (*16*). We compared our estimates of the size-resolved atmospheric dust load with previously published results from Kok *et al.* (*16*), and with an ensemble of AeroCom models [Aerosol Comparison between Observations and Models project—GISS, Global Ozone Chemistry Aerosol Radiation and Transport (GOCART), Community Atmosphere Model (CAM), Model for Atmospheric Transport and Chemistry (MATCH), Model for OZone And Related chemical Tracers (MOZART), IMPACT, Laboratoire d'Optique Atmo-sphérique (LOA); see Materials and Methods and section S2 for details] representing the collective state of commonly used global atmospheric models (*16*, *19*). It is worth noting that the ensemble of AeroCom models used for comparison is different from the ensemble of global models used to constrain the dust size distributions (see table S3).

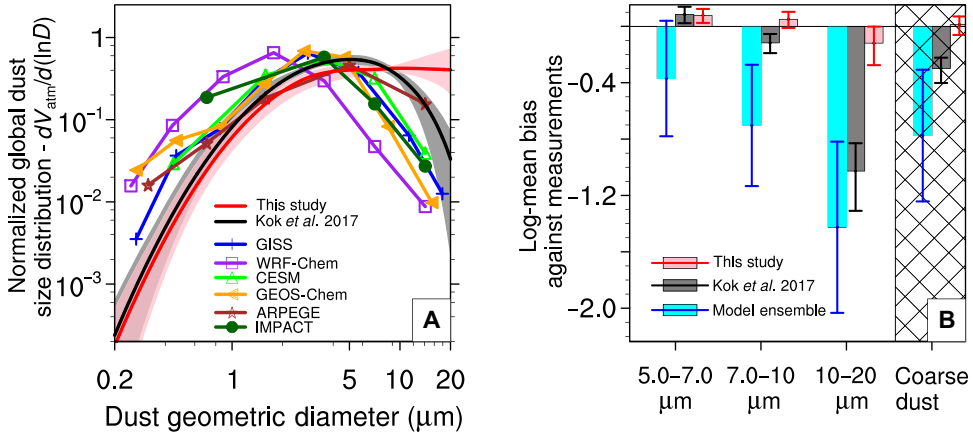

Fig. 1. Constraints on the global coarse dust size distribution. (**A**) Constraint on the global dust size distribution obtained using measurements of atmospheric dust size distributions (red/pink) indicates that the atmosphere contains substantially more coarse dust than obtained in a recent analysis (black/gray; (*16*)) and accounted for in an ensemble of global model simulations (colored lines). Each size distribution is normalized such that the integral of *dV*/*dD* equals one. (**B**) Size-resolved log-mean bias against measurements of dust size distribution (see also Fig. 2) indicates that our constraints on the coarse dust size distribution perform better than those obtained from Kok *et al.* (*16*) (black/gray) and an ensemble of global model simulations (blue/cyan; global models used are shown in Fig. 1A). The last column shows the overall log-mean bias for all coarse dust between diameter 5 and 20 μm. The shading in (A) and the error bars in (B) represent the 95% confidence interval.

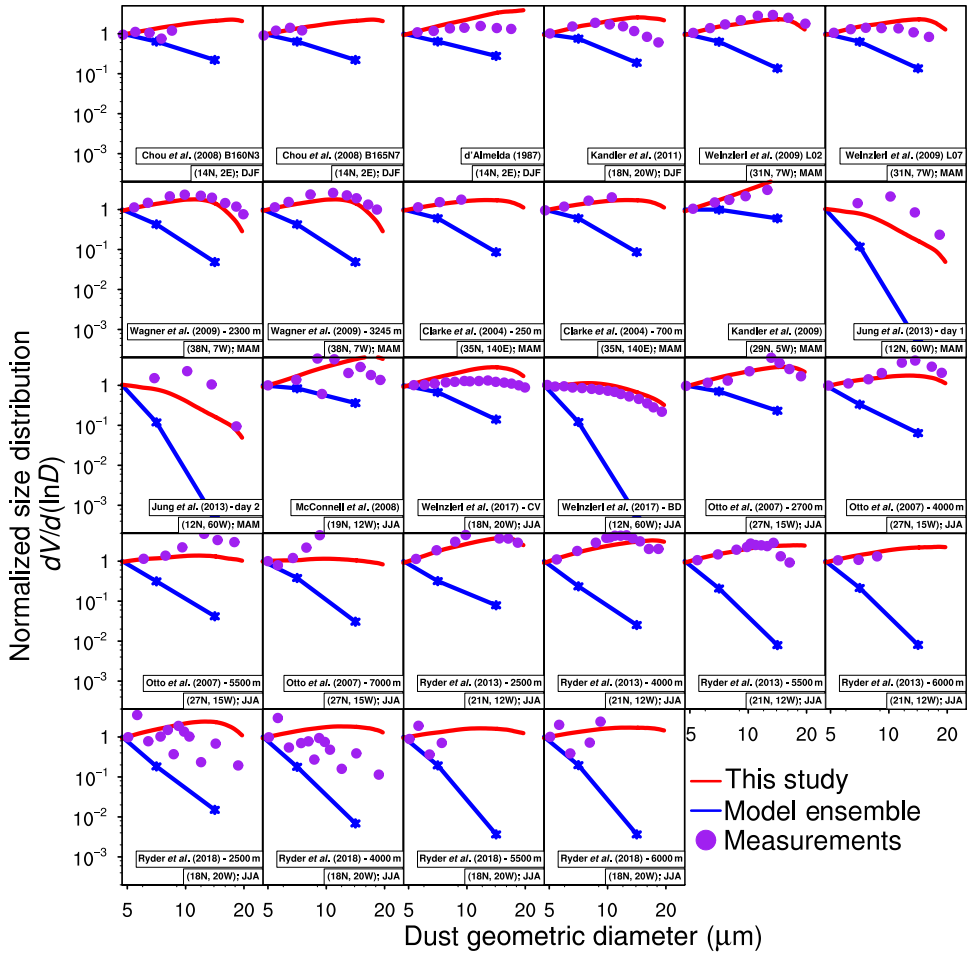

Fig. 2. Measurement compilation of coarse dust size distributions indicates that current global models substantially underestimate coarse dust fractions. We compare each measurement [purple dots; compiled by (*18*)] against the corresponding seasonally averaged dust size distribution obtained from an ensemble of model simulations (blue lines) as well as from this study (red lines). All size distributions are normalized at 5-μm diameter to emphasize the discrepancies.

We find that current models miss most of the coarse dust load in the atmosphere (Fig. 3). That is, the atmosphere contains about 17 Tg (10 to 29 Tg) of coarse dust, whereas AeroCom models account for only 4.0 Tg (3.5 to 6.0 Tg), thus missing about three-quarters of the coarse dust load in the atmosphere. In addition to the missing coarse dust, current models do not account for giant dust particles with $D > 20$ μm, which can contribute substantially to mass loading close to source regions (*6*). As a result, we consider our estimates of the coarse dust load in the atmosphere to be lower bound (*20*), and the underestimation of coarse dust in AeroCom models may, thus, be even larger than we estimate here. Furthermore, a recent analysis of the atmospheric dust load from Kok *et al.* (*16*) that used constraints of the emitted dust size distribution also substantially underestimates the coarse dust load, accounting for only 10 Tg (6 to 15 Tg) of the coarse dust load. Because this recent analysis (*16*) and the AeroCom models miss most of the coarse dust, they also attribute the aerosol optical depth produced by coarse dust to fine dust instead, resulting in an overestimation of fine dust (Fig. 3). Overall, the global atmosphere contains about 40% more dust (fine and coarse) than what is simulated by AeroCom models, and that is about 80% of the total mass load of particulate matters in the atmosphere (*22*).

Possible reasons for why models miss most of the coarse dust

The systematic underestimation of atmospheric coarse dust suggests that one or more important processes are inaccurately represented in global atmospheric models. Since the atmospheric dust size distribution is primarily determined by the size distribution of dust at emission and size-dependent deposition processes (*2*, *19*), our results suggest that models inadequately represent either the size distribution at emission or deposition processes and possibly both (Fig. 2). To improve size distribution at emission, most of the model simulations in our ensemble used a coarser dust size distribution at emission (*16*), which is based on experimental constraints following brittle fragmentation theory (*23*), than those used in AeroCom models (*19*). However, recent measurements taken over the Sahara desert suggest that these global models still underestimate the coarse dust at emission (*24*). Moreover, several previously published measurements of emitted size distribution may have also underestimated the coarse dust particles because of the losses of particles in the instrument's inlet system (*25*). Even when the emitted dust size distribution is constrained using measurements (*16*, *23*), the comparison of globally averaged dust size distributions in Figs. 1 and 3 suggests that coarse dust also deposits out of the atmosphere less quickly than

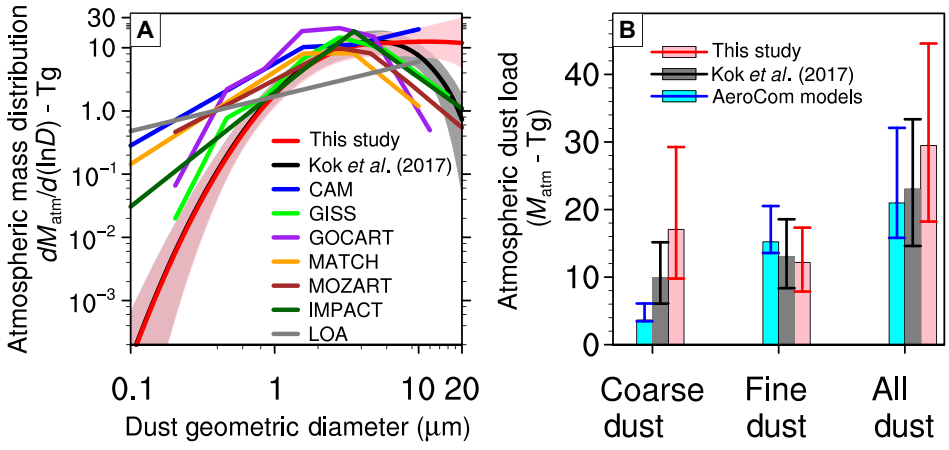

Fig. 3. Constraints on the mass of dust in the atmosphere. (**A**) Size-resolved dust mass distribution (Tg) indicates that the mass of dust in the atmosphere (red/pink) is significantly more than those obtained from (*16*) (black/gray) or an ensemble of AeroCom models obtained from (*19*) (colored lines/cyan bars), and (**B**) shows the corresponding atmospheric dust load (Tg) integrated for the coarse dust (D = 5.0 to 20 μm), fine dust (D = 0.1 to 5.0 μm), and all dust (D = 0.1 to 20 μm). The shading in (A) and the error bars in (B) represent the 95% confidence interval.

predicted in models. This finding is supported by measurements that found coarse dust particles are deposited at greater distances from dust-source regions than can be predicted by models or explained by current dust deposition theory (*5*, *12*). Our results further indicate that dust deposits too quickly in models, because model biases are larger relative to measurements taken farther from dust sources than those taken closer to dust sources (see table S2). In addition, satellite-based retrievals and ship-based measurements of dust optical depth across the dust-dominated parts of the North Atlantic indicate that the height of dust layers decreases more slowly away from dust sources than has been simulated by a range of climate models (*4*). Although inaccuracies in the emitted dust size distributions likely contribute to the underestimation of coarse dust in models, a range of measurements indicates that the underestimation of atmospheric coarse dust is also driven by too fast deposition of coarse dust in global models.

Several possible reasons could contribute to global models depositing coarse dust out of the atmosphere too quickly. First, models assume dust is spherical (*26*), which likely causes an overestimation of their gravitational settling speed. The rationale for this is that aspherical dust particles have a greater surface-to-volume ratio and, thus, a slower deposition velocity than spherical dust. Second, turbulent or convective vertical mixing within an elevated dust layer such as the Sahara Air Layer can work against gravitational settling, therefore increasing the lifetime of the coarse dust in the atmosphere (*27*). This convective mixing can be generated either by strong horizontal winds that induce vertical wind shear and buoyancy around the transporting dust (*28*) or by differential vertical radiative heating within the dust layer (*29*). Unlike at the TOA, dust particles can radiatively warm a dust layer in the SW and cool it in the LW (*29*). Therefore, more coarse dust in a dust layer can lead to a stronger LW cooling at the top and a stronger SW warming at the lower part, inducing a vertical mixing that can keep the dust layer elevated farther from source regions than what global models predict. The potential for this vertical mixing is supported by observational evidence that includes the lack of variability with height in both the measured aerosol concentration (*5*, *9*) and the satellite-retrieved depolarization ratio (*30*) within the dust layer, as well as vertically uniform radiosonde-derived potential temperature profiles retrieved within the dust layer (*9*) over the North Atlantic.

A third reason for why models overestimate dust deposition could be that charged dust particles in the atmosphere generate vertical electrical forces that can potentially counteract gravitational settling (*31*). While some measurements have shown evidence of electrically charged dust particles in the atmosphere (*32*), and even proposed it as a mechanism for coarse dust particles persisting for long distance over the Mediterranean region (*33*), it remains unclear whether this mechanism could substantially contribute to the missing coarse dust in global models (*27*). Fourth, global models can also overestimate dust deposition because of excessive numerical diffusion due to the type of advective scheme used for dust transport (*4*, *26*). For example, (*26*) showed that not accounting for second-order derivatives in the numerical scheme could cause an overestimation of the dust deposition, resulting in an underestimation of the atmospheric dust load by a factor of two. However, by increasing model resolutions, errors associated with numerical diffusion can be reduced, although not eliminated (*34*). Last, the uncertainty in the simulated vertical distribution and the numerical representation of the number of bins used during dust transport may also contribute to the missing coarse dust in global models (*35*, *36*). For example, if dust plumes in global models simulate a lower starting altitude than observed or use too few bins or modes to transport the dust particles, it could result in a faster deposition of coarse dust in the models (*4*, *36*). Together, dust asphericity, convective mixing within the dust layer, levitation of charged dust, and uncertainties in simulated dust vertical distribution and numerical representation may all contribute to the underestimation of coarse dust in global models.

Implications of the missing coarse dust

Our finding that most of the coarse dust particles are missing in global models indicates that these models underestimate the extent of various important impacts of coarse dust on the Earth system. First, global models underestimate the radiative impact coarse dust has on the global climate because it underestimates the amount of coarse dust in the atmosphere. Since coarse dust warms by absorbing both SW and LW radiation (*16*), the underestimation of coarse dust by

both climate models and the recent analysis of Kok *et al.* (*16*) indicate that the net dust direct radiative effect (DRE) is more warming than has been previously estimated. To better understand the impact of the missing coarse dust on the global climate, we obtain constraints on the global dust DRE at the TOA. We do so by combining constraints on the size-resolved global dust optical depth obtained using the constraints on the atmospheric dust load (Fig. 3) and modeling constraints on the size-resolved dust radiative effect efficiency—which is the simulated dust DRE at the TOA per unit dust aerosol optical depth (see Materials and Methods). We find that coarse dust produces a TOA warming that is substantially larger than is simulated in current models and estimated from past analyses (Fig. 4) (*16*). Specifically, the TOA warming due to coarse dust is 0.20 $W{\cdot}m^{-2}$ (0.11 to 0.36 $W{\cdot}m^{-2}$), whereas the ensemble of AeroCom models accounts for only 0.04 $W{\cdot}m^{-2}$ (0.01 to 0.09 $W{\cdot}m^{-2}$). This larger TOA warming by coarse dust in our estimate is driven in large part by increased extinction of LW radiation, although increased extinction of SW radiation also plays a role (see figs. S4 and S5). Similarly, since the global estimates from Kok *et al.* (*16*) use constraints that leverage only the measurements of the emitted dust size distribution, a 7.0 Tg (1.8 to 14.9 Tg) underestimation of the coarse dust load results in a 0.07 $W{\cdot}m^{-2}$ (0.00 to 0.20 $W{\cdot}m^{-2}$) underestimation of the coarse dust warming of the global climate. In contrast to the coarse dust warming, our result indicates less TOA cooling by fine dust because the increased extinction from coarse dust necessitates less extinction from fine dust to match satellite constraints on dust aerosol optical depth (*21*). Therefore, accounting for coarse dust in the atmosphere causes the net impact of dust at the TOA to be substantially less cooling than previously estimated, resulting in an increased likelihood (about 40%) that dust net warms the global climate (Fig. 3).

Our analysis of dust DRE is subject to some limitations that affect the estimated TOA warming by the missing coarse dust (see also section S5). For instance, our estimate of dust DRE is limited by the uncertainties in the simulated size-resolved dust radiative effect efficiencies (see Materials and Methods and section S5). In particular, a recent study (*37*) suggests that the dust refractive index used in the model simulations of the radiative effect efficiency might overestimate the imaginary part of the refractive index in the LW spectrum. As such, our estimate of dust DRE may overestimate the coarse dust warming in the LW. On the other hand, although we limit our analysis to dust with $D \leq 20$ μm because of a dearth of both size distribution measurements and model simulations that extend to larger particle sizes (see Materials and Methods), giant dust particles with $D > 20$ μm have been observed to contribute substantially to dust concentrations and LW extinction close to major source regions such as the Sahara desert (*20*). As such, the underestimation of TOA coarse dust warming in AeroCom models may also be larger than we estimated here. Further measurement and modeling constraints on dust properties are, thus, needed to better estimate the radiative effects of coarse and giant dust particles in the atmosphere.

A second consequence of the coarse dust missing from global models is that the missing coarse dust can bias the simulations of global clouds and precipitation. Since the absorption of SW radiation by coarse dust warms the atmosphere (*29*), an underestimation of the warming coarse dust within a cloud layer could cause an underestimation of cloud evaporation that can suppress precipitation (*14*). In addition, SW absorption may also result in enhanced precipitation through its impact on large-scale dynamics (*38*). In contrast, coarse dust is an important source of giant cloud condensation nuclei, the presence of which can accelerate the formation of precipitation by producing large cloud droplets (*15*, *39*). Therefore, the underestimation of coarse dust by global models can substantially affect the amount and timing of precipitation.

A third consequence of the coarse dust missing from global models is an underestimation of dust deposition into the ocean. Since more coarse dust particles are present in the atmosphere, it also suggests that they have a longer lifetime than those simulated in global models. Whereas current global models simulate a substantial amount of dry deposition over land and close to source regions (*36*), a longer coarse dust lifetime increases coarse dust deposition farther

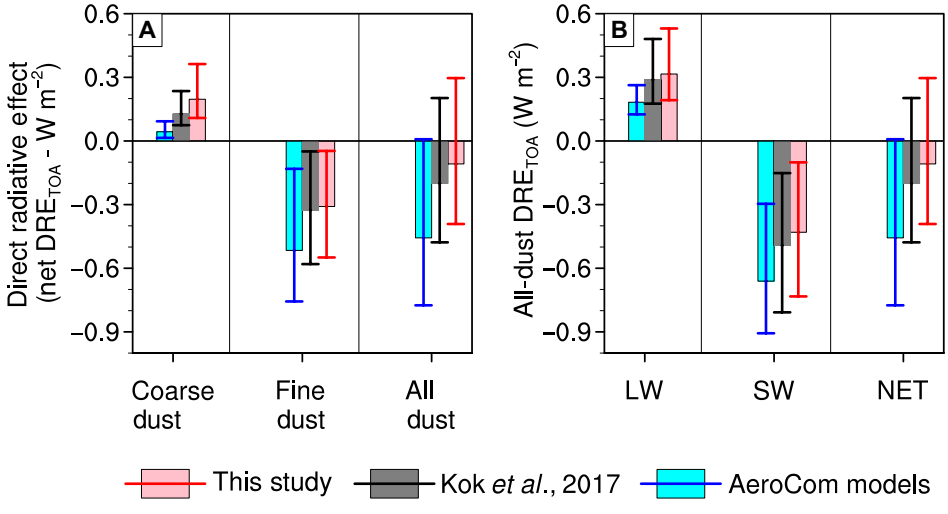

Fig. 4. Constraints on dust direct radiative effects at the top of the atmosphere (DRE$_{TOA}$ W·m^{-2}). Size-aggregated DRE$_{TOA}$ indicates that accounting for the missing coarse dust increases the coarse dust warming, resulting in an overall reduction in the global all-dust radiative cooling. The DRE$_{TOA}$ ($W{\cdot}m^{-2}$) values are obtained in this study (red/pink), from Kok *et al.* (*16*) (black/gray), and an ensemble of AeroCom models (blue lines). (**A**) DRE$_{TOA}$ values for the coarse dust (D = 5.0 to 20 μm), fine dust (D = 0.1 to 5.0 μm), and all dust (D = 0.1 to 20 μm). (**B**) All-dust DRE$_{TOA}$ values for longwave (LW) and shortwave (SW) components and the net (LW + SW). The error bars represent the 95% confidence interval.

from dust sources and into the nearby oceans. Therefore, accounting for the missing coarse dust in global models will increase dust deposition into the ocean, thus also increasing dust-induced productivity of ocean ecosystems and the uptake of carbon dioxide into the deep ocean (*11*, *13*).

CONCLUSIONS

We have shown that climate models miss most of the coarse dust ($D \geq 5$ μm) in the atmosphere, causing an underestimation of important impacts of coarse dust on ocean ecosystems, clouds, and global climate. We find that the mass of coarse dust in the atmosphere is about four times greater than simulated in current climate models, resulting in greater total dust mass load in the atmosphere. Although inaccuracies in the representation of dust emission might contribute to this underestimation of coarse dust in models, our results indicate that climate models also deposit coarse dust out of the atmosphere too quickly. Accounting for this missing coarse dust increases the TOA coarse dust warming by about 0.15 $W{\cdot}m^{-2}$ (0.10 to 0.24 $W{\cdot}m^{-2}$), increases the fertilization of ocean ecosystems by dust deposition, and affects the distribution of global clouds and precipitation. Therefore, climate models must account for the missing coarse dust to accurately simulate its impact on clouds, biogeochemistry, and global climate.

MATERIALS AND METHODS

To estimate the amount of coarse dust particles in the atmosphere, we developed a framework that combines an ensemble of model simulations with a compilation of dozens of in situ dust size distributions. We describe this framework below and use it to obtain constraints on the globally averaged dust size distribution and the global load of coarse dust. We also estimate the impact of this global load of coarse dust on the global dust DRE.

Constraining the global dust size distribution

We constrained the global coarse dust size distribution by determining the size-dependent globally representative correction factor needed to bring model simulations in optimal agreement with a compilation of measured atmospheric dust size distributions. Specifically, we determined the correction factor for each particle bin by minimizing the sum of the squared deviations between the modeled and the measured coarse dust size distributions. That is

$$\chi_k^2(D) = \sum_{j=1}^{N_o} \left\{ \log\left[\delta_{atm}^k(D) \cdot \frac{d\widehat{V_f^{k,j}}}{dD}(D) \right] - \log\left[\frac{d\widehat{V_o^j}}{dD}(D) \right] \right\}^2 \quad (1)$$

First, $\frac{d\widehat{V_o^j}}{dD}$ is the j^{th} measured dust size distribution, and N_o is the total number of available measurements. We give a summary of these measured atmospheric dust size distributions in the Supplementary Materials (section S1), but details can be found elsewhere in (*18*) and the references therein. Second, the $\frac{d\widehat{V_f^{k,j}}}{dD}$ is the modeled dust size distribution that is obtained from the simulated dust mass fraction of model k. These models include the GISS ModelE atmospheric general circulation model—GISS, WRF-Chem, CESM, GEOS-Chem, ARPEGE-Climat (from the Centre National de Recherches Météorologiques Earth system model), and IMPACT (see section S2). Furthermore, each $\frac{d\widehat{V_f^{k,j}}}{dD}$ corresponds to the location, height, and season of each j^{th} measurement (fig. S1). Although each measurement often represents an average of several days or months, here we compare them to the corresponding modeled seasonally averaged size distribution (Fig. 2). Such a comparison is possible because the monthly or submonthly variability of the normalized modeled dust size distribution for each season is often small (*2*). We also compared Eq. 1 in the logarithmic space because the size distributions often span several orders of magnitude (*2*). Last, δ_{atm}^k is the size-resolved correction factor needed to bring each model simulation, k, in optimal agreement with the compilation of measured dust size distributions. We use six models to describe the state of dust size distributions in global atmospheric model simulations (see the summary of the climate model simulations in section S2 and table S3).

To estimate the correction factor (δ_{atm}^k), both the modeled and measured dust size distributions must be on the same equal footing concerning the particle bin resolution—that is, D in Eq. 1 must be the same for both modeled and measured dust size distributions. Therefore, we define a common bin spacing spanning the diameter range covered by each measurement, and we estimate the corresponding size distribution that is mapped onto these new particle bins (see details of the procedure in section S3). That is, $\frac{d\widehat{V_o^j}}{dD}$ is the size distribution that maps the j^{th} measurements (O^j) to the new particle bins, and $\frac{d\widehat{V_f^{k,j}}}{dD}$ is the corresponding size distribution that maps the simulated dust mass fraction ($f^{k,j}$) from model k to the new particle bins. These common particle bins are defined by diameter D_i, such that $i = 1, \ldots, N_j$, and N_j is the total number of bins for the diameter range of the j^{th} measurement. We set the coarse dust diameters for $D_i \geq 5$ μm since this represents the diameter at which most models begin to underestimate the coarse dust (*16*). In addition, we limit the maximum particle diameter to $D_{max} = 20$ μm, following some recent studies (*16*, *18*) and for a better comparison with global models, since most models do not simulate particles larger than D_{max}. Although dust particles with a diameter larger than 20 μm have been measured in the atmosphere especially close to dust source regions (*6*, *20*, *40*), they are relatively limited and, therefore, constraints on the global load of dust with $D_i > D_{max}$ would be highly uncertain (*2*).

We next obtained constraints on the global coarse dust size distribution in the atmosphere by solving Eq. 1 for the size-dependent correction factor that each model needs to minimize the deviation from the compilation of the in situ measurements. That is

$$\left.\frac{dV_{atm}^k}{dD}(D_i)\right|_{global} = \left.\frac{d\widehat{V}_f^k}{dD}(D_i)\right|_{global} \cdot \delta_{atm}^k(D_i) \quad (2)$$

where $\left.\frac{dV_{atm}^k}{dD}\right|_{global}$ is the constraint on the global atmospheric dust size distribution that corrects for the missing coarse dust for each model simulation k, and $\left.\frac{d\widehat{V}_f^k}{dD}(D_i)\right|_{global}$ is the globally averaged dust size distribution from model simulationk k. Similar to $\frac{d\widehat{V}_f^k}{dD}$, we also estimate the sub-bin distributions of $\left.\frac{d\widehat{V}_f^k}{dD}(D_i)\right|_{global}$ for each model, mapping it to the common particle bin resolution with diameter D_i (see section S3.2). One difficulty in obtaining the correction factor δ_{atm}^k and the

global dust size distribution $\left.\frac{dV^k_{atm}}{dD}\right|_{global}$ in Eq. 2 above are the differences in the measured size ranges, which may result in discontinuities in δ^k_{atm} and $\left.\frac{dV^k_{atm}}{dD}\right|_{global}$ estimates. To avoid this problem, we fit a generalized theoretical function (see Eq. 6 in (*18*)) that describes the atmospheric dust size distribution to the resulting global dust size distribution.

The procedure above obtained constraints on the global coarse dust size distribution by using measurement constraints of atmospheric size distribution only for dust particles with $D \geq 5$ μm (Eq. 2). However, knowledge of both coarse dust ($D_i \geq 5$ μm) and fine dust ($D_i < 5$ μm) are necessary to estimate the total dust atmospheric load and the dust direct radiative impact. Therefore, we use the existing constraints on global fine dust size distribution from Kok *et al.* (*16*), which leveraged measurements of emitted size distributions with modeling and experimental constraints on dust size distribution. We do so because this global fine dust size distribution from Kok *et al.* (*16*) was used in Adebiyi *et al.* (*18*), and the corresponding estimates of dust size distribution accurately reproduce the in situ measurements for fine dust particles between $D_i = 0.5$ to 5 μm [see Fig. 4 in (*18*)]. We, thus, obtained the complete dust size distribution for dust diameter D_i between $D_{min} = 0.1$ μm and $D_{max} = 20$ μm by combining the fine dust size distribution from Kok *et al.* (*16*) with the above constraints on the coarse dust size distribution (Eq. 2) (see Fig. 1A).

Obtaining the atmospheric dust load and the direct dust radiative effect

Using the constrained globally averaged dust size distribution, we estimated the atmospheric dust load and the direct dust radiative effect that accounts for the missing coarse dust, following the methodology described in Kok *et al.* (*16*). First, we estimated the size-resolved global atmospheric dust mass load (M_{atm}) by combining constraints on the global dust size distribution $\frac{dV_{atm}}{dD}$ with constraints on dust aerosol optical depth (τ_{atm}) and dust mass extinction efficiency (ε_{atm}) at 550-nm wavelength

$$\frac{dM_{atm}(D)}{dD} = A_{Earth} \cdot \frac{\tau_{atm}}{\varepsilon_{atm}} \cdot \frac{dV_{atm}(D)}{dD} \quad (3)$$

where A_{Earth} is the area of Earth and $\frac{dV_{atm}}{dD}$ is obtained from Eq. 2 above. We obtained τ_{atm} from (*21*), which observationally constrained the global τ_{atm} using satellite and ground-based measurements supplemented with an ensemble of global model simulations, yielding $\tau_{atm} = 0.030 \pm 0.005$. The dust mass extinction efficiency is calculated using the constrained global dust size distribution ($\frac{dV_{atm}}{dD}$) from Eq. 2, the density of dust ($\rho_d = 2.5 \pm 0.2$ g cm^{-3}), and the dust extinction efficiency (Q_{ext}). Unlike the estimation of dust extinction efficiency in climate models that use spherical assumption for dust shape, here we obtained Q_{ext} from Kok *et al.* (*16*), which leveraged measurements of globally averaged dust index of refraction and accounts for dust asphericity based on observation of dust aspect ratio and height-to-width ratio. Using this constraint on Q_{ext}, we estimate ε_{atm} as

$$\varepsilon_{atm} = \int_{D_{min}}^{D_{max}} \frac{dV_{atm}(D)}{dD} \frac{3}{2\rho_d D} Q_{ext}(D) dD \quad (4)$$

Second, we use the constraint on the global atmospheric dust mass load ($\frac{dM_{atm}}{dD}$; Eq. 3) and the dust extinction efficiency (Q_{ext}) to estimate the size-resolved global direct dust radiative effect R_{TOA} at the TOA—R_{TOA}, following (*16*). That is

$$R_{TOA}(D) = \frac{1}{A_{Earth}} \int_{D_{min}}^{D_{max}} \frac{d\tau_d(D)}{dD} \Omega_{TOA}(D)\, dD \quad (5)$$

and

$$\frac{d\tau_d(D)}{dD} = \frac{dM_{atm}(D)}{dD} \frac{3}{2\rho_d D} Q_{ext}(D)$$

From the equation, $\frac{d\tau_d}{dD}$ is the constraint on the size-resolved global dust aerosol optical depth, and Ω_{TOA} is the size-resolved globally averaged all-sky TOA radiative effect efficiency—which is the dust radiative effect that a dust particle with diameter D produces per unit dust aerosol optical depth. Both R_{TOA} and Ω_{TOA} are defined for the SW and the LW spectra as $R_{TOA} = R_{TOA,\,SW} + R_{TOA,\,LW}$ and $\Omega_{TOA} = \Omega_{TOA,\,SW} + \Omega_{TOA,\,LW}$. We obtained Ω_{TOA} values using four global model simulations from Kok *et al.* (*16*). These models include GISS, WRF-Chem, CESM, and GEOS-Chem. Details of the dust optical properties, including the refractive indices, used in estimating Ω_{TOA} both in the SW and LW can be found in Kok *et al.* (*16*) (see also section S2 and table S3).

Since the particle bins of the model simulations are discretized, we have to also discretize R_{TOA} in Eq. 5, such that

$$R_{TOA}(D_{\gamma,i}) = \sum_{i=1}^{N_\gamma} \frac{\Omega^\gamma_{TOA}(D_{\gamma,i})}{A_{Earth}} \int_{D_{\gamma,i,-}}^{D_{\gamma,i,+}} \frac{d\tau_d(D)}{dD} dD \quad (6)$$

where $D_{\gamma,i,-}$ and $D_{\gamma,i,+}$ are, respectively, the lower and upper diameter limits of particle bin i, with $i = 1,\ldots,N_\gamma$, N_γ is the total number of bins for each of the four global model simulation γ. It is worth noting here that the climate model simulations γ used to constrain R_{TOA} in Eq. 6 are different from the model simulations k used to constrain the globally averaged dust size distribution in Eq. 2 above (see section S2 and table S3). Last, the estimation of corresponding dust load and DRE for AeroCom models follows the description in Kok *et al.* (*16*) and summarized in section S4.

Quantifying the uncertainties

We quantified the uncertainties in the globally averaged dust size distribution ($\frac{dV_{atm}}{dD}$; Eq. 2), the size-resolved global dust load ($\frac{dM_{atm}}{dD}$; Eq. 3), and the dust DRE (R_{TOA}; Eq. 6) using a nonparametric procedure based on the bootstrap method. To do so, we assumed that the sets of input variables for each equation are independent and are defined by probability distributions. Therefore, using these probability distributions, we can estimate the resulting probability distribution of $\frac{dV_{atm}}{dD}$, $\frac{dM_{atm}}{dD}$, and R_{TOA}, by randomly sampling (with replacement) each of the input variables for a large number of times (10^4). Sampling with replacement implies that the same realization can be selected from the probability distribution multiple times or not selected at all.

Although our nonparametric procedure propagates the uncertainties in the observations and model simulations, our result is still affected by other limitations associated with the input parameters (see section S5). As a result, our estimates of coarse dust can further be improved as more measurements of dust size distribution, and accurate constraints on other dust properties become available.

SUPPLEMENTARY MATERIALS

Supplementary material for this article is available at http://advances.sciencemag.org/cgi/content/full/6/15/eaaz9507/DC1

REFERENCES AND NOTES

1. S. Kinne, M. Schulz, C. Textor, S. Guibert, Y. Balkanski, S. E. Bauer, T. Berntsen, T. F. Berglen, O. Boucher, M. Chin, W. Collins, F. Dentener, T. Diehl, R. Easter, J. Feichter, D. Fillmore, S. Ghan, P. Ginoux, S. Gong, A. Grini, J. Hendricks, M. Herzog, L. Horowitz, I. Isaksen, T. Iversen, A. Kirkevåg, S. Kloster, D. Koch, J. E. Kristjansson, M. Krol, A. Lauer, J. F. Lamarque, G. Lesins, X. Liu, U. Lohmann, V. Montanaro, G. Myhre, J. E. Penner, G. Pitari, S. Reddy, O. Seland, P. Stier, T. Takemura, X. Tie, An AeroCom initial assessment – optical properties in aerosol component modules of global models. *Atmos. Chem. Phys.* **6**, 1815–1834 (2006).
2. N. Mahowald, S. Albani, J. F. Kok, S. Engelstaeder, R. Scanza, D. S. Ward, M. G. Flanner, The size distribution of desert dust aerosols and its impact on the Earth system. *Aeolian Res.* **15**, 53–71 (2014).
3. J. W. Hurrell, M. M. Holland, P. R. Gent, S. Ghan, J. E. Kay, P. J. Kushner, J.-F. Lamarque, W. G. Large, D. Lawrence, K. Lindsay, W. H. Lipscomb, M. C. Long, N. Mahowald, D. R. Marsh, R. B. Neale, P. Rasch, S. Vavrus, M. Vertenstein, D. Bader, W. D. Collins, J. J. Hack, J. Kiehl, S. Marshall, J. W. Hurrell, M. M. Holland, P. R. Gent, S. Ghan, J. E. Kay, P. J. Kushner, J.-F. Lamarque, W. G. Large, D. Lawrence, K. Lindsay, W. H. Lipscomb, M. C. Long, N. Mahowald, D. R. Marsh, R. B. Neale, P. Rasch, S. Vavrus, M. Vertenstein, D. Bader, W. D. Collins, J. J. Hack, J. Kiehl, S. Marshall, The community earth system model: A framework for collaborative research. *Bull. Am. Meteorol. Soc.* **94**, 1339–1360 (2013).
4. A. Ansmann, F. Rittmeister, R. Engelmann, S. Basart, O. Jorba, C. Spyrou, S. Remy, A. Skupin, H. Baars, P. Seifert, F. Senf, T. Kanitz, Profiling of Saharan dust from the Caribbean to western Africa – Part 2: Shipborne lidar measurements versus forecasts. *Atmos. Chem. Phys.* **17**, 14987–15006 (2017).
5. B. Weinzierl, A. Ansmann, J. M. Prospero, D. Althausen, N. Benker, F. Chouza, M. Dollner, D. Farrell, W. K. Fomba, V. Freudenthaler, J. Gasteiger, S. Groß, M. Haarig, B. Heinold, K. Kandler, T. B. Kristensen, O. L. Mayol-Bracero, T. Müller, O. Reitebuch, D. Sauer, A. Schäfler, K. Schepanski, A. Spanu, I. Tegen, C. Toledano, A. Walser, The saharan aerosol long-range transport and aerosol–cloud-interaction experiment: Overview and selected highlights. *Bull. Am. Meteorol. Soc.* **98**, 1427–1451 (2017).
6. C. L. Ryder, F. Marenco, J. K. Brooke, V. Estelles, R. Cotton, P. Formenti, J. B. McQuaid, H. C. Price, D. Liu, P. Ausset, P. D. Rosenberg, J. W. Taylor, T. Choularton, K. Bower, H. Coe, M. Gallagher, J. Crosier, G. Lloyd, E. J. Highwood, B. J. Murray, Coarse-mode mineral dust size distributions, composition and optical properties from AER-D aircraft measurements over the tropical eastern Atlantic. *Atmos. Chem. Phys.* **18**, 17225–17257 (2018).
7. J. M. Prospero, E. Bonatti, C. Schubert, T. N. Carlson, Dust in the Caribbean atmosphere traced to an African dust storm. *Earth Planet. Sci. Lett.* **9**, 287–293 (1970).
8. D. L. Westphal, O. B. Toon, T. N. Carlson, A two-dimensional numerical investigation of the dynamics and microphysics of Saharan dust storms. *J. Geophys. Res.* **92**, 3027–3049 (1987).
9. E. Jung, B. Albrecht, J. M. Prospero, H. H. Jonsson, S. M. Kreidenweis, Vertical structure of aerosols, temperature, and moisture associated with an intense African dust event observed over the eastern Caribbean. *J. Geophys. Res. Atmos.* **118**, 4623–4643 (2013).
10. P. R. Betzer, K. L. Carder, R. A. Duce, J. T. Merrill, N. W. Tindale, M. Uematsu, D. K. Costello, R. W. Young, R. A. Feely, J. A. Breland, R. E. Bernstein, A. M. Greco, Long-range transport of giant mineral aerosol particles. *Nature* **336**, 568–571 (1988).
11. T. D. Jickells, Z. S. An, K. K. Andersen, A. R. Baker, G. Bergametti, N. Brooks, J. J. Cao, P. W. Boyd, R. A. Duce, K. A. Hunter, H. Kawahata, N. Kubilay, J. laRoche, P. S. Liss, N. Mahowald, J. M. Prospero, A. J. Ridgwell, I. Tegen, R. Torres, Global iron connections between desert dust, ocean biogeochemistry, and climate. *Science* **308**, 67–71 (2005).
12. M. van der Does, L. F. Korte, C. I. Munday, G.-J. A. Brummer, J.-B. W. Stuut, Particle size traces modern Saharan dust transport and deposition across the equatorial North Atlantic. *Atmos. Chem. Phys.* **16**, 13697–13710 (2016).
13. T. Jickells, P. Boyd, K. A. Hunter, in *Mineral Dust* (Springer, Dordrecht, 2014), pp. 359–384.
14. A. Nenes, B. Murray, A. Bougiatioti, in *Mineral Dust* (Springer Netherlands, Dordrecht, 2014), pp. 287–325.
15. V. A. Karydis, A. P. Tsimpidi, S. Bacer, A. Pozzer, A. Nenes, J. Lelieveld, Global impact of mineral dust on cloud droplet number concentration. *Atmos. Chem. Phys.* **17**, 5601–5621 (2017).
16. J. F. Kok, D. A. Ridley, Q. Zhou, R. L. Miller, C. Zhao, C. L. Heald, D. S. Ward, S. Albani, K. Haustein, Smaller desert dust cooling effect estimated from analysis of dust size and abundance. *Nat. Geosci.* **10**, 274–278 (2017).
17. B. H. Samset, C. W. Stjern, E. Andrews, R. A. Kahn, G. Myhre, M. Schulz, G. L. Schuster, Aerosol absorption: Progress towards global and regional constraints. *Curr. Clim. Chang. Reports.* **4**, 65–83 (2018).
18. A. Adebiyi, J. Kok, Y. Wang, A. Ito, D. A. Ridley, P. Nabat, C. Zhao, Dust constraints from joint observational-modelling-experimental analysis (DustCOMM): Comparison with measurements and model simulations. *Atmos. Chem. Phys. Discuss.*, 1–57 (2019).
19. N. Huneeus, M. Schulz, Y. Balkanski, J. Griesfeller, J. Prospero, S. Kinne, S. Bauer, O. Boucher, M. Chin, F. Dentener, T. Diehl, R. Easter, D. Fillmore, S. Ghan, P. Ginoux, A. Grini, L. Horowitz, D. Koch, M. C. Krol, W. Landing, X. Liu, N. Mahowald, R. Miller, J.-J. Morcrette, G. Myhre, J. Penner, J. Perlwitz, P. Stier, T. Takemura, C. S. Zender, Global dust model intercomparison in AeroCom phase i. *Atmos. Chem. Phys.* **11**, 7781–7816 (2011).
20. C. L. Ryder, E. J. Highwood, A. Walser, P. Seibert, A. Philipp, B. Weinzierl, Coarse and giant particles are ubiquitous in saharan dust export regions and are radiatively significant over the sahara. *Atmos. Chem. Phys. Discuss.* **19**, 1–36 (2019).
21. D. A. Ridley, C. L. Heald, J. F. Kok, C. Zhao, An observationally constrained estimate of global dust aerosol optical depth. *Atmos. Chem. Phys.* **16**, 15097–15117 (2016).
22. C. Textor, M. Schulz, S. Guibert, S. Kinne, Y. Balkanski, S. Bauer, T. Berntsen, T. Berglen, O. Boucher, M. Chin, F. Dentener, T. Diehl, J. Feichter, D. Fillmore, P. Ginoux, S. Gong, A. Grini, J. Hendricks, L. Horowitz, P. Huang, I. S. A. Isaksen, T. Iversen, S. Kloster, D. Koch, A. Kirkevåg, J. E. Kristjansson, M. Krol, A. Lauer, J. F. Lamarque, X. Liu, V. Montanaro, G. Myhre, J. E. Penner, G. Pitari, M. S. Reddy, Ø. Seland, P. Stier, T. Takemura, X. Tie, The effect of harmonized emissions on aerosol properties in global models – an AeroCom experiment. *Atmos. Chem. Phys.* **7**, 4489–4501 (2007).
23. J. F. Kok, A scaling theory for the size distribution of emitted dust aerosols suggests climate models underestimate the size of the global dust cycle. *Proc. Natl. Acad. Sci.* **108**, 1016–1021 (2011).
24. P. D. Rosenberg, D. J. Parker, C. L. Ryder, J. H. Marsham, L. Garcia-Carreras, J. R. Dorsey, I. M. Brooks, A. R. Dean, J. Crosier, J. B. McQuaid, R. Washington, Quantifying particle size and turbulent scale dependence of dust flux in the Sahara using aircraft measurements. *J. Geophys. Res. Atmos.* **119**, 7577–7598 (2014).
25. G. Fratini, P. Ciccioli, A. Febo, A. Forgione, R. Valentini, Size-segregated fluxes of mineral dust from a desert area of northern China by eddy covariance. *Atmos. Chem. Phys.* **7**, 2839–2854 (2007).
26. P. Ginoux, Effects of nonsphericity on mineral dust modeling. *J. Geophys. Res.* **108**, 4052 (2003).
27. M. van der Does, P. Knippertz, P. Zschenderlein, R. Giles Harrison, J.-B. W. Stuut, The mysterious long-range transport of giant mineral dust particles. *Sci. Adv.* **4**, eaau2768 (2018).
28. P. Knippertz, M. C. Todd, Mineral dust aerosols over the Sahara: Meteorological controls on emission and transport and implications for modeling. *Rev. Geophys.* **50**, RG1007 (2012).
29. T. N. Carlson, S. G. Benjamin, Radiative heating rates for saharan dust. *J. Atmos. Sci.* **37**, 193–213 (1980).
30. J. Gasteiger, S. Groß, D. Sauer, M. Haarig, A. Ansmann, B. Weinzierl, Particle settling and vertical mixing in the Saharan Air Layer as seen from an integrated model, lidar, and in situ perspective. *Atmos. Chem. Phys.* **17**, 297–311 (2017).
31. Z. Ulanowski, J. Bailey, P. W. Lucas, J. H. Hough, E. Hirst, Alignment of atmospheric mineral dust due to electric field. *Atmos. Chem. Phys.* **7**, 6161–6173 (2007).
32. K. A. Nicoll, R. G. Harrison, Z. Ulanowski, Observations of Saharan dust layer electrification. *Environ. Res. Lett.* **6**, 014001 (2011).
33. J.-B. Renard, F. Dulac, P. Durand, Q. Bourgeois, C. Denjean, D. Vignelles, B. Couté, M. Jeannot, N. Verdier, M. Mallet, In situ measurements of desert dust particles above the western Mediterranean Sea with the balloon-borne Light Optical Aerosol Counter/sizer (LOAC) during the ChArMEx campaign of summer 2013. *Atmos. Chem. Phys.* **18**, 3677–3699 (2018).
34. M. J. Prather, X. Zhu, S. E. Strahan, S. D. Steenrod, J. M. Rodriguez, Quantifying errors in trace species transport modeling. *Proc. Natl. Acad. Sci. U.S.A.* **105**, 19617–19621 (2008).
35. S. Generoso, I. Bey, M. Labonne, F.-M. Bréon, Aerosol vertical distribution in dust outflow over the Atlantic: Comparisons between GEOS-Chem and Cloud-Aerosol Lidar and Infrared Pathfinder Satellite Observation (CALIPSO). *J. Geophys. Res.* **113**, D24209 (2008).
36. K. Schepanski, I. Tegen, A. Macke, Saharan dust transport and deposition towards the tropical northern Atlantic. *Atmos. Chem. Phys.* **9**, 1173–1189 (2009).
37. C. Di Biagio, P. Formenti, Y. Balkanski, L. Caponi, M. Cazaunau, E. Pangui, E. Journet, S. Nowak, S. Caquineau, M. O. Andreae, K. Kandler, T. Saeed, S. Piketh, D. Seibert, E. Williams, J.-F. Doussin, Global scale variability of the mineral dust long-wave refractive index: A new dataset of in situ measurements for climate modeling and remote sensing. *Atmos. Chem. Phys.* **17**, 1901–1929 (2017).
38. K. M. Lau, K. M. Kim, Y. C. Sud, G. K. Walker, A GCM study of the response of the atmospheric water cycle of West Africa and the Atlantic to Saharan dust radiative forcing. *Ann. Geophys.* **27**, 4023–4037 (2009).
39. J. T. Kelly, C. C. Chuang, A. S. Wexler, Influence of dust composition on cloud droplet formation. *Atmos. Environ.* **41**, 2904–2916 (2007).
40. C. L. Ryder, E. J. Highwood, T. M. Lai, H. Sodemann, J. H. Marsham, Impact of atmospheric transport on the evolution of microphysical and optical properties of Saharan dust. *Geophys. Res. Lett.* **40**, 2433–2438 (2013).
41. J. M. Haywood, S. Osborne, P. N. Francis, A. Keil, P. Formenti, M. O. Andreae, P. H. Kaye, The mean physical and optical properties of regional haze dominated by biomass burning aerosol measured from the C-130 aircraft during SAFARI 2000. 108, 10.1029/2002JD002226, (2003).

42. A. D. Clarke, Size distributions and mixtures of dust and black carbon aerosol in Asian outflow: Physiochemistry and optical properties. *J. Geophys. Res.* **109**, 15S09 (2004).
43. S. Otto, M. de Reus, T. Trautmann, A. Thomas, M. Wendisch, S. Borrmann, Atmospheric radiative effects of an in situ measured Saharan dust plume and the role of large particles. *Atmos. Chem. Phys.* **7**, 4887–4903 (2007).
44. S. R. Osborne, B. T. Johnson, J. M. Haywood, A. J. Baran, M. A. J. Harrison, C. L. McConnell, Physical and optical properties of mineral dust aerosol during the Dust and Biomass-burning Experiment. *J. Geophys. Res.* **113**, 00C03 (2008).
45. C. Chou, P. Formenti, M. Maille, P. Ausset, G. Helas, M. Harrison, S. Osborne, Size distribution, shape, and composition of mineral dust aerosols collected during the African Monsoon Multidisciplinary Analysis Special Observation Period 0: Dust and Biomass-Burning Experiment field campaign in Niger, January 2006. *J. Geophys. Res.* **113**, 00C10 (2008).
46. C. L. McConnell, E. J. Highwood, H. Coe, P. Formenti, B. Anderson, S. Osborne, S. Nava, K. Desboeufs, G. Chen, M. A. J. Harrison, Seasonal variations of the physical and optical characteristics of Saharan dust: Results from the Dust Outflow and Deposition to the Ocean (DODO) experiment. *J. Geophys. Res.* **113**, 14S05 (2008).
47. B. Weinzierl, A. Petzold, M. Esselborn, M. Wirth, K. Rasp, K. Kandler, L. Schütz, P. Koepke, M. Fiebig, Airborne measurements of dust layer properties, particle size distribution and mixing state of Saharan dust during SAMUM 2006. *Tellus B Chem. Phys. Meteorol.* **61**, 96–117 (2009).
48. F. Wagner, D. Bortoli, S. Pereira, M. J. Costa, A. M. Silva, B. Weinzierl, M. Esselborn, A. Petzold, K. Rasp, B. Heinold, I. Tegen, Properties of dust aerosol particles transported to Portugal from the Sahara desert. *Tellus B Chem. Phys. Meteorol.* **61**, 297–306 (2009).
49. K. Kandler, L. SchüTZ, C. Deutscher, M. Ebert, H. Hofmann, S. Jäckel, R. Jaenicke, P. Knippertz, K. Lieke, A. Massling, A. Petzold, A. Schladitz, B. Weinzierl, A. Wiedensohler, S. Zorn, S. Weinbruch, Size distribution, mass concentration, chemical and mineralogical composition and derived optical parameters of the boundary layer aerosol at Tinfou, Morocco, during SAMUM 2006. *Tellus B Chem. Phys. Meteorol.* **61**, 32–50 (2009).
50. K. Kandler, K. Lieke, N. Benker, C. Emmel, M. Küpper, D. Müller-Ebert, M. Ebert, D. Scheuvens, A. Schladitz, L. Schütz, S. Weinbruch, Electron microscopy of particles collected at Praia, Cape Verde, during the Saharan Mineral Dust Experiment: Particle chemistry, shape, mixing state and complex refractive index. *Tellus B Chem. Phys. Meteorol.* **63**, 475–496 (2011).
51. G. A. D'Almeida, L. Schutz, Number, mass and volume distributions of mineral aerosol and soils of the Sahara. *J. Clim. Appl. Meteorol.* **22**, 233–243 (1983).
52. X. Li, H. Maring, D. Savoie, K. Voss, J. M. Prospero, Dominance of mineral dust in aerosol light-scattering in the North Atlantic trade winds. *Nature* **380**, 416–419 (1996).
53. S.-M. Li, J. Tang, H. Xue, D. Toom-Sauntry, Size distribution and estimated optical properties of carbonate, water soluble organic carbon, and sulfate in aerosols at a remote high altitude site in western China. *Geophys. Res. Lett.* **27**, 1107–1110 (2000).
54. H. Maring, D. L. Savoie, M. A. Izaguirre, C. McCormick, R. Arimoto, J. M. Prospero, C. Pilinis, Aerosol physical and optical properties and their relationship to aerosol composition in the free troposphere at izaña, tenerife, canary islands, during July 1995. *J. Geophys. Res. Atmos.* **105**, 14677–14700 (2000).
55. T. W. Andreae, M. O. Andreae, C. Ichoku, W. Maenhaut, J. Cafmeyer, A. Karnieli, L. Orlovsky, Light scattering by dust and anthropogenic aerosol at a remote site in the Negev desert, Israel. *J. Geophys. Res.* **107**, AAC3-1–AAC33-18 (2002).
56. P. K. Quinn, D. J. Coffman, T. S. Bates, T. L. Miller, J. E. Johnson, E. J. Welton, C. Neusüss, M. Miller, P. J. Sheridan, Aerosol optical properties during INDOEX 1999: Means, variability, and controlling factors. *J. Geophys. Res.* **107**, INX219-1–INX219-25 (2002).
57. J. S. Reid, H. H. Jonsson, H. B. Maring, A. Smirnov, D. L. Savoie, S. S. Cliff, E. A. Reid, J. M. Livingston, M. M. Meier, O. Dubovik, S.-C. Tsay, Comparison of size and morphological measurements of coarse mode dust particles from Africa. *J. Geophys. Res.* **108**, 8593 (2003).
58. O. Dubovik, A. Smirnov, B. N. Holben, M. D. King, Y. J. Kaufman, T. F. Eck, I. Slutsker, Accuracy assessments of aerosol optical properties retrieved from Aerosol Robotic Network (AERONET) Sun and sky radiance measurements. *J. Geophys. Res. Atmos.* **105**, 9791–9806 (2000).
59. R. L. Miller, R. V. Cakmur, J. Perlwitz, I. V. Geogdzhayev, P. Ginoux, D. Koch, K. E. Kohfeld, C. Prigent, R. Ruedy, G. A. Schmidt, I. Tegen, Mineral dust aerosols in the NASA Goddard Institute for Space Sciences ModelE atmospheric general circulation model. *J. Geophys. Res.* **111**, D06208 (2006).
60. C. Zhao, S. Chen, L. R. Leung, Y. Qian, J. F. Kok, R. A. Zaveri, J. Huang, Uncertainty in modeling dust mass balance and radiative forcing from size parameterization. *Atmos. Chem. Phys.* **13**, 10733–10753 (2013).
61. M. Michou, P. Nabat, D. Saint-Martin, Development and basic evaluation of a prognostic aerosol scheme (v1) in the CNRM Climate Model CNRM-CM6. *Geosci. Model Dev.* **8**, 501–531 (2015).
62. A. Ito, J. F. Kok, Do dust emissions from sparsely vegetated regions dominate atmospheric iron supply to the Southern Ocean? *J. Geophys. Res. Atmos.* **122**, 3987–4002 (2017).
63. A. A. Adebiyi, J. F. Kok, Y. Wang, A. Ito, D. A. Ridley, P. Nabat, C. Zhao, DustCOMM_v1 Input Dataset. *Zenodo* (2019), 10.5281/ZENODO.2620547.
64. S. M. El-Shazly, Studies of the number concentration and size distribution of the suspended dust particles in the atmosphere of Qena/Egypt. *Water Air Soil Pollut.* **45**, 121–133 (1989).
65. C. E. Junge, in *Air chemistry and radioactivity* (Academic Press, 1963), pp. 382–382.
66. L. Martin, C. Mätzler, T. J. Hewison, D. Ruffieux, Intercomparison of integrated water vapour measurements. *Meteorol. Zeitschrift.* **15**, 57–64 (2006).
67. T. Y. Tanaka, M. Chiba, A numerical study of the contributions of dust source regions to the global dust budget. *Glob. Planet. Change.* **52**, 88–104 (2006).
68. H. Maring, D. L. Savoie, M. A. Izaguirre, L. Custals, J. S. Reid, Mineral dust aerosol size distribution change during atmospheric transport. *J. Geophys. Res.* **108**, 8592 (2003).
69. C. A. Friese, M. van der Does, U. Merkel, M. H. Iversen, G. Fischer, J.-B. W. Stuut, Environmental factors controlling the seasonal variability in particle size distribution of modern Saharan dust deposited off Cape Blanc. *Aeolian Res.* **22**, 165–179 (2016).
70. F. E. Volz, Infrared optical constants of ammonium sulfate, sahara dust, volcanic pumice, and flyash. *Appl. Optics* **12**, 564–568 (1973).
71. Y. Fouquart, B. Bonnel, G. Brogniez, J. C. Buriez, L. Smith, J. J. Morcrette, A. Cerf, Y. Fouquart, B. Bonnel, G. Brogniez, J. C. Buriez, L. Smith, J. J. Morcrette, A. Cerf, Observations of saharan aerosols: Results of ECLATS field experiment. Part II: broadband radiative characteristics of the aerosols and vertical radiative flux divergence. *J. Clim. Appl. Meteorol.* **26**, 38–52 (1987).
72. M. Hess, P. Koepke, I. Schult, Optical properties of aerosols and clouds: The software package OPAC. *Bull. Am. Meteorol. Soc.* **79**, 831–844 (1998).
73. C. Di Biagio, P. Formenti, Y. Balkanski, L. Caponi, M. Cazaunau, E. Pangui, E. Journet, S. Nowak, M. O. Andreae, K. Kandler, T. Saeed, S. Piketh, D. Seibert, E. Williams, J.-F. Doussin, Complex refractive indices and single scattering albedo of global dust aerosols in the shortwave spectrum and relationship to iron content and size. *Atmos. Chem. Phys. Discuss.* **19**, 15503–15531 (2019).
74. R. L. Miller, P. Knippertz, C. Pérez García-Pando, J. P. Perlwitz, I. Tegen, in *Mineral Dust* (Springer Netherlands, Dordrecht, 2014), pp. 327–357.
75. G. A. D'Almeida, On the variability of desert aerosol radiative characteristics. *J. Geophys. Res.* **92**, 3017 (1987).

Acknowledgments: We thank Y. Huang and K. Ledger for their comments and discussions. **Funding:** This work was developed with support from the University of California President's Postdoctoral Fellowship awarded to A.A.A. and from the National Science Foundation (NSF) grants 1552519 and 1856389 awarded to J.F.K. **Author contributions:** A.A.A. and J.F.K both designed the research. A.A.A. performed the research and analyzed the data. J.F.K. provided some of the data and discussed the results. A.A.A. wrote the paper. **Competing interests:** The authors declare that they have no competing interests. **Data and materials availability:** All data needed to evaluate the conclusions in the paper are present in the paper and/or the Supplementary Materials, as well as references cited therein. Additional data related to this paper may be requested from the authors.

Submitted 22 October 2019
Accepted 9 January 2020
Published 8 April 2020
10.1126/sciadv.aaz9507

Citation: A. A. Adebiyi, J. F. Kok, Climate models miss most of the coarse dust in the atmosphere. *Sci. Adv.* **6**, eaaz9507 (2020).